

Phase transitions in Rb_2KLuF_6 crystal

A. S. Krylov, A. N. Vtyurin, V. N. Voronov & S. N. Krylova

To cite this article: A. S. Krylov, A. N. Vtyurin, V. N. Voronov & S. N. Krylova (2019) Phase transitions in Rb_2KLuF_6 crystal, *Ferroelectrics*, 538:1, 28-34, DOI: [10.1080/00150193.2019.1569982](https://doi.org/10.1080/00150193.2019.1569982)

To link to this article: <https://doi.org/10.1080/00150193.2019.1569982>



Published online: 17 May 2019.



Submit your article to this journal [↗](#)



View Crossmark data [↗](#)



Phase transitions in Rb_2KLuF_6 crystal

A. S. Krylov, A. N. Vtyurin, V. N. Voronov, and S. N. Krylova

Kirensky Institute of Physics FRC KSC SB RAS, Krasnoyarsk, Russia

ABSTRACT

The Raman spectra of Rb_2KLuF_6 elpasolite crystal have been studied in a wide temperature range, including two phase transitions: from the cubic phase to the tetragonal phase and then to the monoclinic phase. The results of an analysis of the temperature dependences of the parameters of spectral lines are in good agreement with the thermodynamic data on the phase transitions. The analysis of Raman spectra shows that the transition from cubic to tetragonal phase is a second-order transition and the transition from the tetragonal to the monoclinic phase is a weak first-order transition.

ARTICLE HISTORY

Received 14 May 2018

Accepted 31 October 2018

KEYWORDS

Temperature; Raman spectroscopy; elpasolite; phase transition

PACS NUMBER

78.30.Hv; 78.30.-j

1. Introduction

This work is devoted to the analysis of temperature phase transitions in the Rb_2KLuF_6 crystal. The $\text{Rb}_2\text{KB}^{(3+)}\text{F}_6$ crystals belongs to the elpasolite family with common formula $a_2\text{B}^{(1)}\text{B}^{(2)}\text{X}_6$, where a and B are metal cations or more complex molecular ions and X are oxygen anions or halogens. This family of crystals accommodating divalent and trivalent cations in perfect octahedral sites (B) of cubic crystal structure [1–5]. The real cubic crystal structure of haloid elpasolites is unstable. It is because of the instability of real crystal structures these crystals can undergo structural phase transitions or exist in a distorted phase up to the melting temperature. The nature of the transitions is ferroelastic [6–10].

The decreasing the size of the $\text{B}^{(3+)}$ cation leads to the change of the structural phase transitions sequence from one transition $\text{Fm}3\text{m} - \text{P}12_1/\text{n}1$ for $\text{B}^{(3+)} = \text{Ho}, \text{Dy}, \text{Tb}$ to two transitions $\text{Fm}3\text{m} - \text{I}4/\text{m} - \text{P}12_1/\text{n}1$ for $\text{B}^{(3+)} = \text{In}, \text{Sc}, \text{Lu}$ [1]. The transitions in the Rb_2KInF_6 and Rb_2KScF_6 are associated with small rotations of $\text{B}^{(3+)}\text{F}_6$ octahedra and displacements of rubidium atoms. The transitions are the displacement type, which are accompanied by the condensation of a soft phonon mode. The studies of isostructural elpasolites Rb_2KHoF_6 and Rb_2KDyF_6 [7, 11, 12] have shown the first-order phase transition in these crystals. The total entropy change upon transition from the cubic phase to the monoclinic phase depends on the size of the trivalent ion and decreases from 1.3R (Ho) to 0.7R (Sc) [1]. The maximum value (1.3R) is rather large for purely displacive transitions but does not allow to assign these transformations to order-disorder transitions. Therefore, it seems interesting to do new research with other ions of rare-earth elements and analyze the data obtained for several fluorides to explain the mechanisms of phase transitions. The Raman spectroscopy can be an additional

CONTACT S. N. Krylova  slanky@iph.krasn.ru

Color versions of one or more of the figures in the article can be found online at www.tandfonline.com/gfer.

© 2019 Taylor & Francis Group, LLC

powerful tool for studying phase transitions. This method allows one to estimate the role of molecular groups in the phase transition mechanism and character of phase transitions.

2. Experiment

The crystals Rb_2KLuF_6 were synthesized in a solid-phase chemical reaction from a mixture of the fluorides RbF , KF , and LuF_3 taken in the appropriate proportions. The reaction was carried out in sealed platinum ampules in an atmosphere of argon.

Raman scattering spectra of Rb_2KLuF_6 crystal have been studied in the temperature range from 8 K to 390 K. Because of the small sample size, we could not observe polarized Raman spectra. Raman spectra were collected in backscattering geometry, using a triple monochromator Jobin Yvon T64000 Raman spectrometer operating in double subtractive mode then detected by a CCD cooled at 140 K. The spectral resolution for the recorded Stokes side Raman spectra was set to 1 cm^{-1} (this resolution was achieved by using gratings with $1800 \text{ grooves mm}^{-1}$ and $100 \mu\text{m}$ slits). The microscope system based on Olympus BX41 microscope with a $50\times$ objective lens $f=10.6 \text{ mm}$ of NA 0.5 provides a focal spot diameter of about $5 \mu\text{m}$ on the sample. Single-mode argon 514.5 nm of Spectra-Physics Stabilite 2017 Ar^+ laser of 100 mW power (15 mW on the sample) was used as excitation light source. We fitted the spectra using damped harmonic oscillator functions. Approximation of internal mode positions was performed using the dependence which corresponds to decay into two phonons:

$$\Omega(T) = \omega_0 + A \left(1 + \frac{1}{\exp(c\hbar\Omega_{\beta 1}/k_B T) - 1} + \frac{1}{\exp(c\hbar\Omega_{\beta 2}/k_B T) - 1} \right),$$

\hbar , k_B , and c are the reduced Planck constant, the Boltzmann constant, and speed of light, respectively.

3. Discussion and conclusion

The Rb_2KLuF_6 crystal undergoes two structural phase transitions: from the cubic phase to the tetragonal phase at $T_1 = 270 \text{ K}$ ($I114/m$, $Z=2$) and then to the monoclinic phase at $T_2 = 366 \text{ K}$ ($p12_1/n1$, $Z=2$) [13, 14].

Vibrational representation in the cubic phase at Brillouin zone center is:

$$\Gamma_{\text{vibr}}(Fm-3m) = A_{1g}(xx, yy, zz) + E_g(xx, yy, zz) + 2F_{2g}(xz, yz, xy) + F_{1g} + 5E_{1u} + F_{2u} \quad (1)$$

In the tetragonal phase

$$\Gamma_{\text{vibr}}(I114/m) = 3A_g(xx, yy, zz) + 3B_g(xx, yy, xy) + 3E_g(xz, yz) + 5A_u + 6E_u + B_u \quad (2)$$

In the monoclinic phase

$$\Gamma_{\text{vibr}}(P12_1/n1) = 12A_g(xx, yy, zz, xy, yx) + 12B_g(xz, yz, zx, zy) + 18A_u + 18B_u \quad (3)$$

where corresponding components of the Raman scattering tensor are given in brackets.

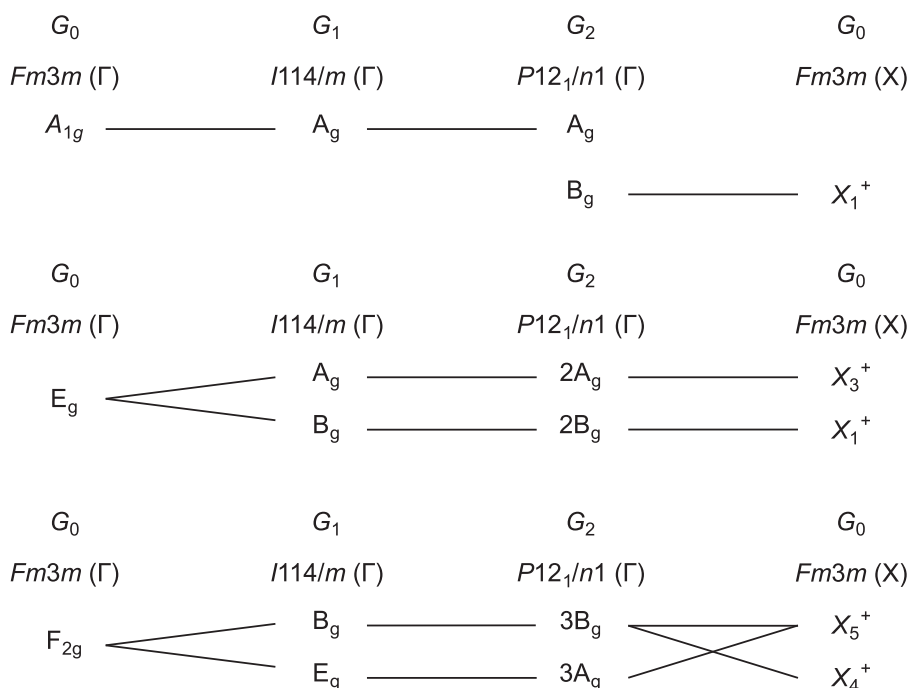


Figure 1. Correlation diagram of the internal vibrational modes of LuF_6 for the cubic, tetragonal and monoclinic symmetries of the elpasolites.

The correlation diagrams of the modes expected in the Raman spectrum are shown in [Figure 1](#). The transition to the monoclinic phase is accompanied by doubling of the unit cell volume. The modes at the $X(0, 0, \pi/a)$ point at the Brillouin zone, including the possible soft mode, are Raman-inactive; however, they can become Raman-active below the second transition point (and the soft mode can also be recovered there). We might even expect further splitting of the modes that are degenerate in the tetragonal phase, including the recovering soft mode corresponding to the transition from the cubic to the tetragonal phase.

The Raman spectra transformation in Rb_2KLuF_6 with temperature is presented in [Figure 2](#). The spectra in the cubic phase (375 K) could be subdivided into four parts, corresponding to vibrations of structural elements: region of lattice vibrations below 100 cm^{-1} ; F–Lu–F bending region, $150\text{--}250\text{ cm}^{-1}$; Lu–F stretching region, $250\text{--}400\text{ cm}^{-1}$, Lu–F stretching (full symmetry vibration), $470\text{--}490\text{ cm}^{-1}$. We could not analyze in detail the behavior of the E_g symmetry Lu–F stretching mode. [Table 1](#) shows assignments and experimental band positions for Rb_2KLuF_6 , Rb_2KScF_6 , Rb_2KInF_6 , Rb_2KHoF_6 , Rb_2KDyF_6 in the cubic phase. In the cubic phase of Rb_2KLuF_6 , stable above $T=370\text{ K}$, three lines are observed at 484 , 210 , and 62 cm^{-1} ([Figure 2](#)) The vibrational frequencies 484 and 210 cm^{-1} correspond to the internal vibrations of LuF_6 octahedra. The frequency of the only active lattice mode in the Raman spectrum is 62 cm^{-1} at 375 K . Experimental band positions for Rb_2KLuF_6 crystal are slightly different from those for Rb_2KScF_6 , Rb_2KInF_6 , Rb_2KHoF_6 , Rb_2KDyF_6 . One can see a narrowing of the lines mentioned above. [Figure 2](#) demonstrates the appearance of additional lines at low temperatures. This feature is in good agreement with the selection rules.

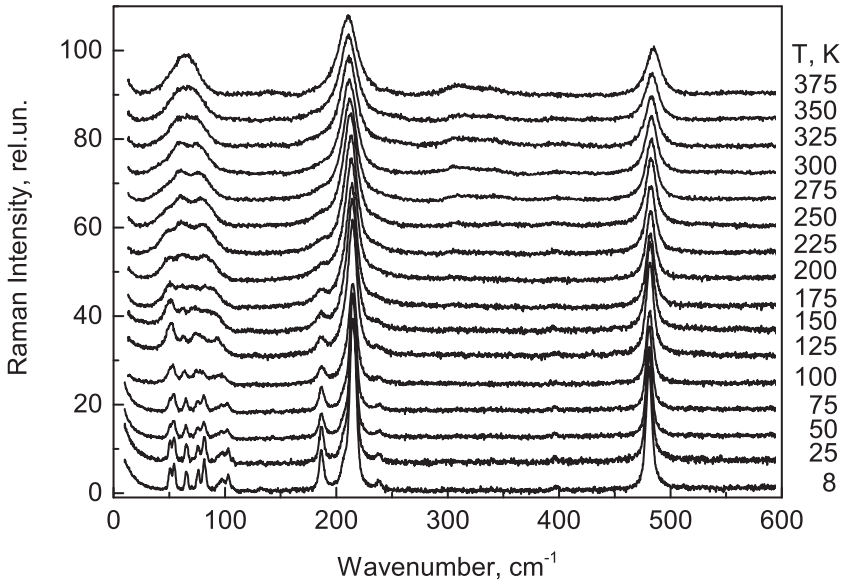


Figure 2. Temperature transformation of Rb_2KLuF_6 Raman spectra.

Table 1. The assignments, band positions in the cubic phase of the $\text{Rb}_2\text{KB}^{(3+)}\text{F}_6$.

Symmetry type	[this work] Rb_2KLuF_6 cm^{-1}	[6] Rb_2KHoF_6 cm^{-1}	[6] Rb_2KDyF_6 cm^{-1}	[7] Rb_2KScF_6 cm^{-1}	[8] Rb_2KInF_6 cm^{-1}	[9] Rb_2KYF_6 cm^{-1}
A_{1g}	484	472	470	505	507	470
E_g			380	390	379	
F_{2g}	210	204	202	230	218	210
F_{2g}	62	61	65	89	69	60

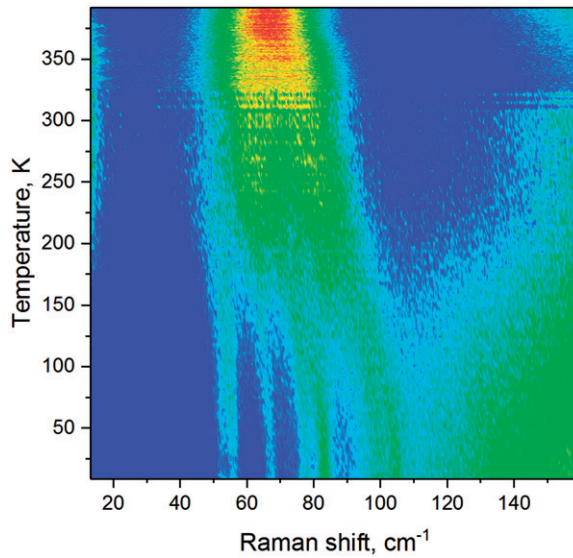


Figure 3. Raman intensity map of Rb_2KLuF_6 crystal in the low wavenumber region.

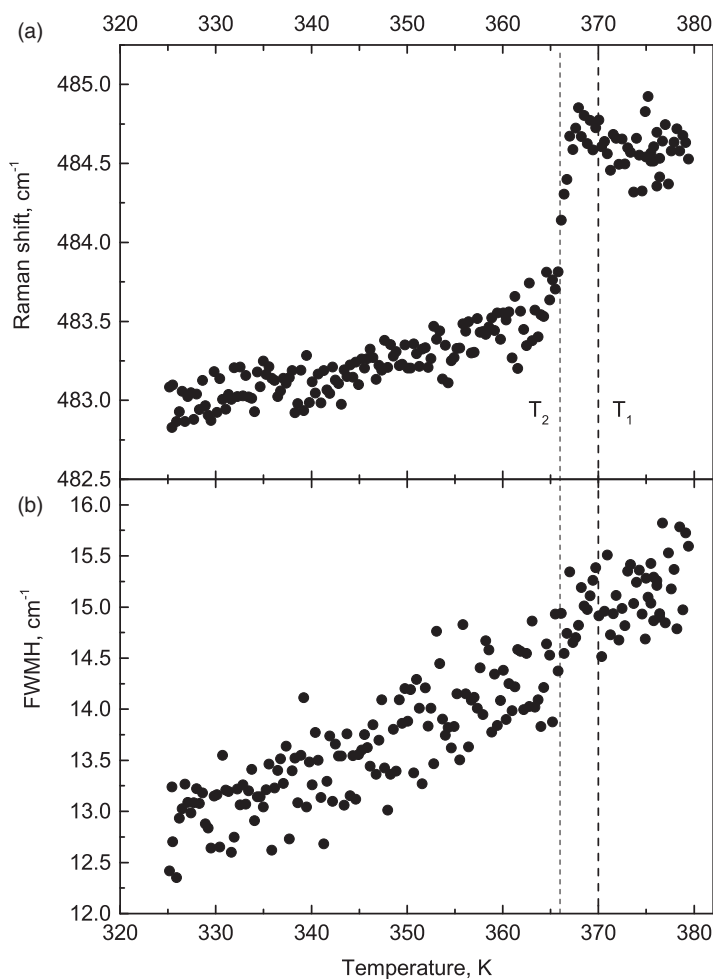


Figure 4. Temperature dependence of the A_{1g} symmetry internal mode: a – position, b – line width (Full Width on Half Maximum).

The behavior of low wavenumber lines at cooling is presented in Figure 3. It is Raman intensity map in the low wavenumber region from red (high intensity of line) to blue (low intensity). The new lines appear lower phase transition temperatures in the Rb_2KLuF_6 . One can see some anomalies of the behavior of Raman lines with temperature. We think that all splitting of the lines are connected with this phase transition. The appearance of new lines is connected with doubling of the volume of the primitive cell. In the low-frequency part of the Raman spectra, a soft mode is not observed. It can be connected with the coupling of the Rb modes with rotational processes of the LuF_6 octahedra.

The temperature dependence of the peak position of the internal mode (A_{1g} symmetry) and FWHM of the line is given in Figure 4. The previous investigations of the temperature phase transitions in Rb_2KScF_6 , Rb_2KInF_6 , Rb_2NaYF_6 crystals showed that full symmetry mode does not change with temperature [8, 9, 15]. However, in our experiment, one can see the abrupt change of the line position (483 cm^{-1}) behavior at

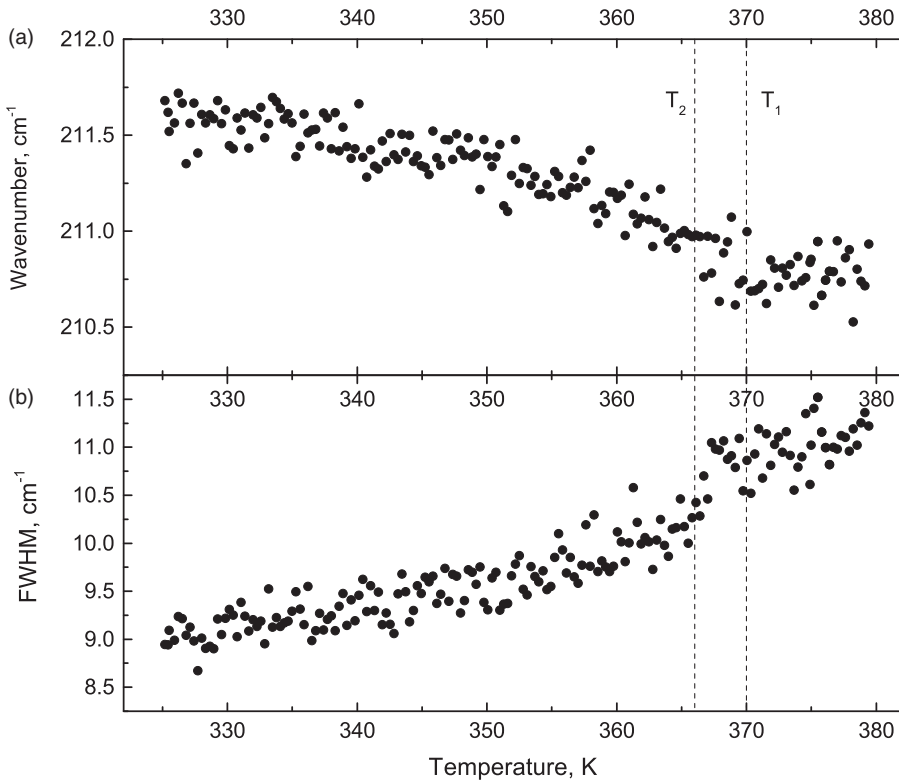


Figure 5. Temperature dependence of the F_{2g} symmetry internal mode: a – position, b – line width (Full Width on Half Maximum).

the 367 K in Rb_2KLuF_6 (Figure 4(a)). Due to the continuous character of line width (Full Width on Half Maximum), we may conclude that it is a weak first-order transition, i.e., nearly continuous (Figure 4(b)).

Temperature dependences of the line position and the width in the region of internal F_{2g} mode are given in Figure 5(a,b). The position of the line changes from 211.5 to 210.5 cm^{-1} under cooling. Two new lines appear below phase transition temperature at 186 and 237 cm^{-1} on both sides of the strong peak at 210 cm^{-1} (Figure 1). Line width decreases under cooling and changes the slope of the curve in the region of phase transitions (Figure 5(b)). According to Raman rules, we can expect splitting of triple degenerated (F_{1g}) Raman active lattice mode and three modes can go from X point of the Brillouin zone. Some lines are very weak, and we can see these lines only at low temperature.

The analysis of the spectral anomalies is performed. It shows that transition from cubic to tetragonal phase has second-order character. The transition from tetragonal to monoclinic phase has a weak first-order character. The phase transition at $T_1 = 270$ K in Rb_2KLuF_6 crystals is due to rotations of the LuF_6 octahedron. The second phase transition in Rb_2KLuF_6 crystals is due to displacement of Rb ions and the rotation LuF_6 octahedron. The small values of the line half-widths and their temperature dependences indicate that the vibration damping in the high-symmetry phase is determined by the decay of phonons due to their anharmonicity and is not related to structure disordering.

Disclosure statement

No potential conflict of interest was reported by the authors.

Funding

This work was partly supported by Russian Foundation for Basic Research Grant no 16-02-00102, 18-02-00754.

References

- [1] I. N. Flerov *et al.*, Ferroelastic phase transitions in fluorides with cryolite and elpasolite structures, *Crystallogr. Rep.* **49**(1), 100 (2004). DOI: [10.1134/1.1643969](https://doi.org/10.1134/1.1643969).
- [2] A. S. Aleksandrovsky *et al.*, Luminescence spectra of Ho³⁺ in distorted parity-breaking HoF₆ – octahedra, *J. Lumin.* **132**(3), 690 (2012). DOI: [10.1016/j.jlumin.2011.11.005](https://doi.org/10.1016/j.jlumin.2011.11.005).
- [3] M. A. Buñuel *et al.*, Luminescence of In³⁺ in Ce³⁺ and Tb³⁺-doped elpasolite-type fluoroindates, *J. Appl. Phys.* **86**(9), 5045 (1999). DOI: [10.1063/1.371477](https://doi.org/10.1063/1.371477).
- [4] L. Cornu *et al.*, Optical contrast and cycling of bistable luminescence properties in Rb₂KIn(1 – x)CexF₆ compounds, *Dalton Trans.* **45**(8), 3380 (2016).
- [5] A. M. Woods *et al.*, Computer modeling of the optical properties of substitutional chromium impurities in halide elpasolites, *J. Phys. Chem. Solids.* **54**(5), 543 (1993). DOI: [10.1016/0022-3697\(93\)90232-G](https://doi.org/10.1016/0022-3697(93)90232-G).
- [6] M. V. Gorev *et al.*, Phase transitions in elpasolites (ordered perovskites), *Mater. Sci. Eng. R: Rep.* **24**(3), 81 (1998). DOI: [10.1016/S0927-796X\(98\)00015-1](https://doi.org/10.1016/S0927-796X(98)00015-1).
- [7] A. Vtyurin *et al.*, Raman scattering and phase transitions in fluorides with elpasolite structure, *Ferroelectrics* **512**(1), 58 (2017).
- [8] S. N. Krylova *et al.*, Lattice dynamics and Raman scattering spectrum of elpasolite Rb₂KScF₆: Comparative analysis, *Phys. Solid State.* **46**(7), 1311 (2004). DOI: [10.1134/1.1778457](https://doi.org/10.1134/1.1778457).
- [9] A. S. Krylov *et al.*, Raman scattering study temperature phase transitions of Rb₂KInF₆ crystal, *Ferroelectrics* **416**(1), 95 (2011). DOI: [10.1080/00150193.2011.577713](https://doi.org/10.1080/00150193.2011.577713).
- [10] M. Couzi, S. Khairoun, and A. Tressaud, Structural phase transitions in Rb₂KM^{III}F₆ elpasolites. Raman scattering and group-theoretical studies of Rb₂KFeF₆ and Rb₂KYF₆, *Phys. Stat. Sol. (a)* **98**(2), 423 (1986). DOI: [10.1002/pssa.2210980213](https://doi.org/10.1002/pssa.2210980213).
- [11] B. V. Beznosikov *et al.*, Structural phase transitions in elpasolites Rb₂NaDyF₆ and Rb₂KDyF₆, *Ferroelectr. Lett. Sect.* **1**, 35 (1983). DOI: [10.1080/07315178308200551](https://doi.org/10.1080/07315178308200551).
- [12] I. N. Flerov *et al.*, Thermodynamic properties of elpasolites Rb₂KB₃F₆ (B³⁺: Er, Ho), *Ferroelectrics.* **168**(1), 55 (1995). DOI: [10.1080/00150199508007848](https://doi.org/10.1080/00150199508007848).
- [13] I. N. Flerov *et al.*, Sequence phase transitions Fm3m–I4/m–P21/n research in Rb₂KInF₆ Rb₂KLuF₆ elpasolites, *Phys. Solid State.* **34**, 3493 (1992).
- [14] V. I. Zinenko, and N. G. Zamkova, Microscopic calculations of displacive (Elpasolite family) and order-disorder (Potassium selenate family) structural phase transitions, *Crystallogr. Rep.* **49**(1), 29 (2004). DOI: [10.1134/1.1643961](https://doi.org/10.1134/1.1643961).
- [15] A. S. Krylov *et al.*, Structural transformations in a single-crystal Rb₂NaYF₆: Raman scattering study, *J. Raman Spectrosc.* **44**(5), 763 (2013). DOI: [10.1002/jrs.4263](https://doi.org/10.1002/jrs.4263).